

Frequency Response from Aggregated V2G Chargers With Uncertain EV Connections

Cormac O'Malley, *Student Member, IEEE*, Luis Badesa, *Member, IEEE*, Fei Teng, *Member, IEEE*, and Goran Strbac, *Member, IEEE*

Abstract—Fast frequency response (FR) is highly effective at securing frequency dynamics after a generator outage in low inertia systems. Electric vehicles (EVs) equipped with vehicle to grid (V2G) chargers could offer an abundant source of FR in future. However, the uncertainty associated with V2G aggregation, driven by the uncertain number of connected EVs at the time of an outage, has not been fully understood and prevents its participation in the existing service provision framework. To tackle this limitation, this paper, for the first time, incorporates such uncertainty into system frequency dynamics, from which probabilistic nadir and steady state frequency requirements are enforced via a derived moment-based distributionally-robust chance constraint. Field data from over 25,000 chargers is analysed to provide realistic parameters and connection forecasts to examine the value of FR from V2G chargers in annual operation of the GB 2030 system. The case study demonstrates that uncertainty of EV connections can be effectively managed through the proposed scheduling framework, which results in annual savings of £6,300 or 37.4 tCO₂ per charger. The sensitivity of this value to renewable capacity and FR delays is explored, with V2G capacity shown to be a third as valuable as the same grid battery capacity.

NOMENCLATURE

Indices and Sets

g, G	Index, Set of generators.
i, I	Index, Set of aggregated EV fleets.
n, N	Index, Set of nodes in the scenario tree.
s, S	Index, Set of storage units.

Constants

Δf_{max}	Maximum admissible frequency deviation (Hz).
$\Delta \tau(n)$	Time-step corresponding to node n (h).
η	V2G charger (dis)charge efficiency.
$\pi(n)$	Probability of reaching node n .
c_{LS}	Value of load-shed from lack of reserve (£/MWh).
ϵ	Acceptable risk of FR under-delivery from V2G.
f_0	Nominal grid frequency (Hz).
μ_i	Mean net EV connection forecast for fleet i .
σ_i	Std of net EV connection forecast for fleet i .
$N_{0,i}$	Current number of connected EVs in fleet i .
$\Delta \tilde{N}_t$	EV connections between t_d and the start of t_s .
$P^d(n)$	Total demand at node n (GW).
$P^w(n)$	Total wind power availability at node n (GW).
$P^{sol}(n)$	Total solar power availability at node n (GW).
$RoCoF_{max}$	Maximum admissible RoCoF (Hz/s).
t_d	Time of scheduling decision (h).
t_s	Scheduling time period (h).
T_{del}	Delay of FR from EVs (s).
T_1	Delivery speed of fast FR (s).
T_2	Delivery speed of slow FR (s).

Decision Variables (continuous unless stated)

b	Binary variable to relax (19).
E_t	Aggregate fleet state of charge at time t (GWh).
H	System inertia after the loss of PL_{max} (GWs).
$P_g(n)$	Power output of units g at node n (GW).
$PLS(n)$	Load-shed from lack of reserve at node n (GW).
$P_s(n)$	Power output from storage s at node n (GW).
$P_i^{EV}(n)$	Power output from EV fleet i at node n (GW).
$P^{wc}(n)$	Wind curtailment at node n (GW).
$P^{solc}(n)$	Solar curtailment at node n (GW).
PL_{max}	Largest power infeed (GW).
R^{ND}	Magnitude of fast FR from non-distributed sources (GW).
R^G	Magnitude of slow FR from thermal plants (GW).
\bar{R}^{EV}	Magnitude of scheduled fast FR from all system V2G chargers (GW).

Linear Expressions of Decision Variables (Deterministic)

$C_g(n)$	Operating cost of units g at node n (£).
g_i	Individual EV FR capacity in fleet i (GW).
$R^G(t)$	FR dynamics of thermal plants (GW).
$R^{ND}(t)$	FR dynamics from non-distributed sources (GW).
x	Auxiliary expression for (9).

Linear Expressions of Decision Variables (Stochastic)

v, y, z	Auxiliary expressions for (9) and (18).
$R^{EV}(t)$	FR dynamics of aggregated V2G chargers (GW).
R^{EV}	Magnitude of total available FR from V2G (GW).
R_i^{EV}	Magnitude of available FR from fleet i (GW).
δ	Excess scheduled FR from EVs compared to amount truly available (GW).

Nonlinear Expressions of Decision Variables (Stochastic)

$\Delta f(t)$	Frequency deviation at time t after outage (Hz).
t^*	Time after outage of frequency nadir (s).

Random Variables

ΔN_i	Net EV connections for fleet i between t_d and the time of outage during t_s .
--------------	--

I. INTRODUCTION

DECARBONISED future power systems will be characterised by low inertia due to the displacement of synchronous fossil fuel generators by converter interfaced generation like wind and solar. This makes grid frequency more volatile, thus more challenging to contain within predefined limits.

Post generator outage, frequency response (FR) is activated to provide a net power injection that aims to arrest frequency

decline by restoring the power balance. The required amount of FR depends on the level of system inertia [1], which covers the transient power deficit by extracting kinetic energy stored within the rotating masses of synchronous generators. Previous work [2] has demonstrated that fast FR from converter interfaced resources, like grid batteries is extremely effective at containing frequency nadir, and thus a vital resource to decouple frequency security from synchronous machines.

Large numbers of electric vehicles (EVs) will be present in future systems, with more than 23 million expected on the road in the UK by 2030 [3]. When paired with vehicle to grid (V2G) chargers, their smart control offers an abundant and valuable [4] source of FR. The capacity of this FR is determined by the number of connected EVs, which cannot be known exactly ahead of time. Thus its inclusion makes the dynamic frequency evolution post-outage uncertain.

Current literature only considers FR from V2G connected EVs deterministically [4], [5]. Reference [5] calculates the profit of FR from individual V2G connected EVs by calculating the optimal charging schedule in relation to historical FR prices and real EV connection data in Great Britain (GB). Whereas [4] models EV fleets as a virtual battery that is disconnected during the working day, showing that FR from bidirectional chargers is up to 20 times more valuable than unidirectional chargers. On the other hand, literature that accounts for EV uncertainty [6]–[8] primarily focus on hourly energy requirements, which can only be used to manage slow (and less valuable), steady state ancillary services like reserve.

This paper fills the conspicuous gap, by presenting a stochastic method to unlock the substantial value of fast (delivered within 1s after an outage) response from V2G chargers for enhancing dynamic security. This necessitates considering intra-hour EV connection uncertainties which we characterise here from field EV charging data.

We propose to schedule FR from fleets of EVs with uncertain plugins using distributionally robust chance constraints (DR-CC). These allow low-probability violation of uncertain constraints for a set of possible probability distributions called an ambiguity set. DR-CC finds the balance between stochastic and robust approaches. It leverages distributional information like moment or unimodality knowledge, to result in less conservative results than robust programs, but requires less precise distributional knowledge than stochastic programs. Furthermore, many useful ambiguity sets facilitate highly tractable analytical convex reformulations.

Ambiguity set construction is generally categorised into two distinct approaches, moment based [7]–[12] and statistical distance based [13], [14]. Although some recent work has sought to combine the two [6]. Both approaches have seen widespread application within steady state energy system modelling, primarily to deal with renewable power generation forecast uncertainty [6], [10]–[14].

Recently, moment based DR-CC are also increasingly being employed to deal with the intrinsic uncertainties of aggregated distributed resources (ADRs) [7]–[10]. Reference [7] develops a method for distribution systems to mitigate their renewable power forecast uncertainty via aggregated EV charging. A model predictive control scheduling approach is used, with

uncertain EV charging demands accounted for via moment based DR-CC. DR-CCs are used in [8] to facilitate the provision of fast reserves from aggregated behind-the-meter loads (including EVs and water heaters). Uncertain energy and power constraints on reserve are considered, with the option to exploit distributional unimodality information to tighten the ambiguity set. Reference [9] applies DR-CCs to schedule reserve from aggregated air-conditioning loads with uncertain reserve capacity limits within an optimal power flow problem. Ambiguity sets considering exact and approximate second moment information are used, which result in a Second-Order Cone (SOC) Program and a Semi-Definite Program respectively. Finally, Bachi et al [10] apply the conic reformulation of a two sided linear DR-CC with known second order moments, first derived in [12], to line loading and nodal voltage constraints under uncertain renewable outputs and uncertain ADR energy demand, revealing the impact of network constraints on ADR's bidding strategy in the day ahead electricity markets.

However, the above references only utilise the flexible demand of ADRs (such as EVs) to provide reserve for steady state power balancing. Non consider the ability of ADRs to assist in the dynamic problem of securing frequency in the transient period immediately following the loss of a large generator. In this paper we establish a DR-CC method to optimally schedule FR from aggregated EV fleets. The operator can specify frequency security violation probability, allowing the preferred trade-off between system risk and operational cost reduction to be found. To the best of our knowledge, this is the first work to explicitly evaluate the impact of uncertainty on the value of FR from distributed providers. Although this paper exclusively focuses on EVs, the presented method is also applicable to other ADRs.

The main contributions of this work are:

- 1) To include uncertainty associated with FR provision from aggregated V2G chargers into the system frequency dynamics, from which probabilistic nadir and steady state security frequency requirements are derived.
- 2) To propose a novel, convex moment-based DR-CC on the maximum scheduled FR from V2G chargers, guaranteeing frequency security following a generator outage under future EV connection uncertainty.
- 3) To analyse field EV fleet connectivity data to provide realistic parameters and EV connection forecasts, as well as guide ambiguity set selection.
- 4) To provide new insight, based on simulating the yearly operation of the GB 2030 system, on the the value of FR from V2G and its sensitivity against renewable generation penetration, grid battery penetration, communication delays and uncertainty levels.

This paper is organised as follows: Section II derives a convex formulation for probabilistic frequency security constraints. Field EV fleet connectivity data is analysed in Section III to inform EV connectivity forecasting and parameter selection, whilst Section IV presents case studies exploring the value of FR from aggregated V2G chargers. Section V gives the conclusions.

II. MODELLING OF AGGREGATED V2G CHARGERS IN FREQUENCY DYNAMICS

This section derives frequency security constraints from the dynamic swing equation, which are non-deterministic due to the uncertain FR capacity from V2G chargers. The proposed DR-CC formulation for these constraints is presented, along with the virtual battery model of aggregate fleet charging.

A. Frequency Security Constraints Under Uncertainty

System frequency evolution post generator loss is accurately approximated by the single machine swing equation [15]:

$$\frac{2H}{f_0} \frac{d\Delta f}{dt} = R^{EV}(t) + R^{ND}(t) + R^G(t) - PL_{max} \quad (1)$$

Load damping is neglected as the level in future systems dominated by power-electronics will be much reduced [16].

FR dynamics are modelled as linear ramps, similar to the work in [1], [2], [16], [17]. Detailed dynamic simulations carried out in Section III of [17] show that droop controls can be accurately and conservatively approximated by a ramp. More detailed dynamic models prohibit closed form solutions to (1), necessary in order to derive convex algebraic frequency security constraints.

$$R^{EV}(t) = \begin{cases} \frac{R^{EV}}{T_1} \cdot t & t \leq T_1 \\ R^{EV} & t > T_1 \end{cases}, R^{ND}(t) = \begin{cases} \frac{R^{ND}}{T_1} \cdot t & t \leq T_1 \\ R^{ND} & t > T_1 \end{cases} \quad (2)$$

$$R^G(t) = \begin{cases} \frac{R^G}{T_2} \cdot t & t \leq T_2 \\ R^G & t > T_2 \end{cases} \quad (3)$$

In this paper $T_1 < T_2$. The slower speed models governor controlled FR from thermal plants. The faster speed comes from power-electronic devices, including V2G chargers and non-distributed devices like grid batteries.

Ahead of time, the dynamics of the cumulative FR delivered from V2G chargers is known, but the magnitude is uncertain. Thus, the grid frequency dynamic is also uncertain. For an individual fleet the response capacity is determined by the charging decisions of that fleet (decision variables), and the number of EVs that are connected (random variable):

$$R_i^{EV} = \underbrace{(D_{max,i} - D_i + C_i)}_{g_i} \cdot (N_{0,i} + \Delta N_i) \quad (4)$$

The cumulative magnitude of FR from V2G chargers is:

$$R^{EV} = \sum_{i \in I} R_i^{EV} \quad (5)$$

It is assumed that charging decisions for EVs within the same fleet are uniform. The number of currently connected EVs N_0 is known. The net EVs connected between now and the time of generator outage (ΔN) can be forecasted, but not known exactly in advance. This paper presents a stochastic framework to incorporate FR from aggregated V2G chargers, whilst explicitly limiting the risk of frequency security breach due to potential under-delivery of FR from EVs.

1) *RoCoF Constraint*: The maximum RoCoF occurs at the moment of PL_{max} outage. At this time no response has been delivered so it is deterministic and limited by inertia alone. Constraining the maximum RoCoF is necessary to prevent RoCoF-sensitive protection systems from disconnecting distributed generation and exacerbating the deficit. Setting $t = 0$ in (1) results in:

$$\frac{2|RoCoF_{max}|}{f_0} \cdot H \geq PL_{max} \quad (6)$$

2) *Steady State*: Frequency drop will be arrested if the sum of FR is greater than the largest loss. Ensured to a high certainty with:

$$\mathbb{P} \left[PL_{max} \leq R^{ND} + R^{EV} + R^G \right] \geq 1 - \epsilon \quad (7)$$

3) *Nadir Constraint*: Here it is assumed that the nadir occurs after T_1 ($\approx 1s$) as the extremely low inertia required to breach the frequency limit Δf_{max} ($\approx -0.8Hz$) would violate the RoCoF constraint (6) for realistic power system parameters. The frequency nadir occurs at the instant of zero RoCoF. According to (1) this is:

$$t^* = \frac{(PL_{max} - (R^{ND} + R^{EV})) \cdot T_2}{R^G} \quad (8)$$

It is shown in [2] that by integrating (1) and then substituting in (8), the nadir constraint can be formed as a convex rotated SOC. Thus the post outage frequency drop is contained with high assurance via:

$$\mathbb{P} \left[\underbrace{\left(\frac{H}{f_0} - \frac{(R^{ND} + R^{EV}) \cdot T_1}{4\Delta f_{max}} \right)}_{=z} \underbrace{\frac{R^G}{T_2}}_{=x} \geq \underbrace{\left(\frac{PL_{max} - (R^{ND} + R^{EV})}{2\sqrt{\Delta f_{max}}} \right)^2}_{=y} \right] \geq 1 - \epsilon \quad (9)$$

Finally, the power injection from aggregated chargers may be delayed due to communication or frequency measurement lag. An additional term in the Nadir constraint can account for this [17]:

$$z = \frac{H}{f_0} - \frac{(R^{ND} + R^{EV}) \cdot T_1}{4\Delta f_{max}} - \frac{R^{EV} \cdot 2T_{del}}{4\Delta f_{max}} \quad (10)$$

B. Convex Reformulation of Chance Constraints

The inclusion of response from aggregated EV's within the frequency dynamics make (7) and (9) non deterministic. Therefor they cannot be applied to optimisations within scheduling or market contexts. This severely limits their use and motivates the need for their convex and deterministic reformulation. Making (9) deterministic is challenging as no convex analytical reformulation of a chance constrained SOC currently exists. However, R^{EV} is the only non deterministic parameter within (7) and (9). Thus ensuring frequency security to a given certainty can be achieved by scheduling an amount of response from the chargers that has an equivalent probability of over delivery:

$$\mathbb{P}\left[\bar{\mathbf{R}}^{EV} \leq \sum_{i \in I} \mathbf{R}_i^{EV}\right] \geq 1 - \epsilon \quad (11)$$

$\bar{\mathbf{R}}^{EV}$ replaces \mathbf{R}^{EV} in (7) and (9), making them deterministic. Constraint (11) is linear, hence if the mean and standard deviation of the forecasted number of connected EVs is known, it can be analytically reformulated into a SOC [11]. We start by defining a new scalar random variable:

$$\delta = \bar{\mathbf{R}}^{EV} - \sum_{i \in I} \mathbf{g}_i \cdot (N_{0,i} + \Delta N_i) \quad (12)$$

Note, δ represents the excess scheduled FR compared to the FR actually available. We want this to be negative with high probability. In a deterministic system ΔN_i is known, $\bar{\mathbf{R}}^{EV} = \sum_{i \in I} \mathbf{R}_i^{EV}$ and thus $\delta = 0$.

Substituting (12) into (11):

$$\mathbb{P}\left[\delta \leq 0\right] \geq 1 - \epsilon \quad (13)$$

Assuming independent EV connections between fleets, the mean and standard deviation of δ are:

$$\mu(\delta) = \bar{\mathbf{R}}^{EV} - \sum_{i \in I} \mathbf{g}_i \cdot (N_{0,i} + \mu_i), \quad \sigma(\delta) = \sqrt{\sum_{i \in I} (\mathbf{g}_i \cdot \sigma_i)^2} \quad (14)$$

Subsequently, δ can be scaled to have a zero mean and unit variance via $\delta_n = (\delta - \mu(\delta))/\sigma(\delta)$:

$$\mathbb{P}\left[\delta_n \leq \frac{-\mu(\delta)}{\sigma(\delta)}\right] \geq 1 - \epsilon \quad (15)$$

The true distribution \mathcal{P} of δ_n is ambiguous. The set of possible distributions that \mathcal{P} might belong to is called an ambiguity set (\mathbb{A}), defined by the distributional assumptions made on \mathcal{P} . This paper utilises the distributionally robust analytical reformulations presented in [11], to reformulate (15) into a convex SOC constraint. Constraint satisfaction is guaranteed at least at the specified certainty level, even under the worst case distribution within \mathbb{A} . The analytical reformulation under this conservative guarantee is facilitated by defining a lower bound on \mathcal{P} 's cumulative distribution function ($f_{\mathcal{P}}(k)$):

$$f_{\mathcal{P}}(k) = \inf_{\mathcal{P} \in \mathbb{A}} \mathbb{P}[\delta_n < k] \quad (16)$$

Given that the function of $f_{\mathcal{P}}(k)$ is increasing, it has a well defined inverse $f_{\mathcal{P}}^{-1}(\lambda)$. Constraint (15) can be written as:

$$\frac{-\mu(\delta)}{\sigma(\delta)} \leq f_{\mathcal{P}}^{-1}(1 - \epsilon) \quad (17)$$

A convex SOC after substituting in the moments of δ_n (14):

$$\sqrt{\sum_{i \in I} (\mathbf{g}_i \cdot \sigma_i)^2} \leq \underbrace{\frac{1}{f_{\mathcal{P}}^{-1}(1 - \epsilon)} \cdot \left(\sum_{i \in I} \mathbf{g}_i \cdot (N_{0,i} + \mu_i) - \bar{\mathbf{R}}^{EV} \right)}_v \quad (18)$$

For some instances when risk aversion is high and the standard deviations of ΔN_i are large, constraint (18) can be infeasible. To ensure feasibility during simulation, a binary variable is

TABLE I
EXPRESSIONS FOR $f_{\mathcal{P}}^{-1}(1 - \epsilon)$

Gaussian	$f_{\mathcal{P}}^{-1}(1 - \epsilon) = \Phi^{-1}(1 - \epsilon)$
Unimodal	$f_{\mathcal{P}}^{-1}(1 - \epsilon) = \begin{cases} \sqrt{\frac{4}{9\epsilon} - 1} & \text{for } 0 \leq \epsilon \leq \frac{1}{6} \\ \sqrt{\frac{3(1-\epsilon)}{1+3\epsilon}} & \text{for } \frac{1}{6} \leq \epsilon \leq 1 \end{cases}$
DRO	$f_{\mathcal{P}}^{-1}(1 - \epsilon) = \sqrt{\frac{1-\epsilon}{\epsilon}}$

added to the right hand side. Using the big-M technique, it simultaneously relaxes (18) and constrains $\bar{\mathbf{R}}^{EV}$ to zero.

$$\sqrt{\sum_{i \in I} (\mathbf{g}_i \cdot \sigma_i)^2} \leq v + M_1 \cdot b \quad (19)$$

$$\bar{\mathbf{R}}^{EV} \leq M_2 \cdot (1 - b) \quad (20)$$

The exact form of $f_{\mathcal{P}}^{-1}(\lambda)$ depends on distributional assumptions made about \mathcal{P} . Here, all ambiguity sets assume knowledge of the first two moments of δ . According to (14), this requires the true mean and standard deviation of forecasted EV connection numbers (μ_i, σ_i) for each fleet to be known. Three distinct ambiguity sets are considered:

- 1) Distributionally Robust Optimisation (DRO) - When only the mean and standard deviation of δ are known.
- 2) Unimodal - The distribution of δ_n is assumed to have a single peak. Likely when ΔN_i are themselves unimodal.
- 3) Gaussian - The distribution of δ_n is assumed to be Gaussian. True when ΔN_i are themselves Gaussian.

More statistical information on \mathcal{P} defines tighter ambiguity sets and thus results in a less conservative chance constraint. The distributional assumptions made on δ defines the form of $f_{\mathcal{P}}^{-1}(1 - \epsilon)$, according to the inverse cumulative distribution for the Gaussian case, or probability inequalities for the Unimodal and DRO case. The exact expressions for $f_{\mathcal{P}}^{-1}(1 - \epsilon)$ are shown in Table I.

C. State of Charge and Reserve

Contrary to when scheduling FR from EVs, scheduling charging uses hourly EV connection numbers. These are assumed deterministic and known. This is justified because: 1) As shown in Section IV and [4], an EV's value in highly renewable systems is dominated by its FR provision. Thus, characterising the impact of uncertainty on EV value is unhindered. 2) Despite constraint (18) being fully compatible with charging-under-uncertainty methods (such as that presented in [8]), deterministic EV charging is used here to simplify modelling and increases insight into system operation under (18), the core contribution of the paper.

Here, each EV fleet is modelled as a virtual aggregate battery. All fleets are modelled in the same way, so the subscript i is dropped for notational clarity. A battery's charge rate is equal to the sum of all the individual constituent EVs.

$$\mathbf{P}^{EV} = (N_0 + \Delta \hat{N}_t) \cdot (\mathbf{D} - \mathbf{C}) \quad (21)$$

$\Delta \hat{N}_t$ is the net change in EV numbers between now and the beginning of the scheduling period t . It is deterministic and read into the simulation via a time series. EV connections are

discretized, occurring at the start of each hour, then remaining constant for the entire timestep. This makes $\Delta\hat{N}_t$ different to ΔN in (12), which is a random variable, representing the instantaneous number of EVs connected. This varies within the hour time-step, necessary because response capacity is determined by the instantaneous net power injection capacity of fleets. Whereas a virtual battery's generation and state of charge relate to the averaged connectivity values.

A battery's state of charge at the end of a scheduling period depends on: that period's charge decisions; its parent node's state of charge at the end of the previous timestep (E_{t-1}); and change in charge incurred by EV (dis)connection.

$$E_t = E_{t-1} + (N_0 + \Delta\hat{N}_t) \cdot (\eta C - \frac{1}{\eta} D) + \Delta N_t^{in} E^{in} - \Delta N_t^o E^o \quad (22)$$

Note that ΔN_t^{in} , ΔN_t^o refer to the number of EVs that connect and disconnect at the beginning of timestep t respectively. Thus $\Delta\hat{N}_t$ is their cumulation between now and the scheduling time period $\Delta\hat{N}_T = \sum_{t=1}^T (\Delta N_t^{in} - N_t^o)$. An EV's (dis)connection states of charge (E^o , E^{in}) are assumed known. Note $E^o \geq E^{in}$, thus $E^o - E^{in}$ represents the EV driving energy expenditure.

D. Stochastic Unit Commitment

To ascertain the system value of FR from aggregated EV fleets with V2G chargers, a pre-existing scheduling model is significantly enhanced to optimally co-ordinate charge and generation decisions in light of uncertain future EV connections. This section briefly introduces the advanced stochastic unit commitment (SUC) model.

The SUC model optimally schedules generator and storage actions to provide reserve, response (fast and slow), inertia and energy production under uncertain renewable output. User defined quantiles of the random variable of net demand (demand net of wind power) are used to construct a scenario tree. Reference [18] demonstrates that well chosen quantiles that branch only at the root node can discretize the continuous range of potential wind realisations in an accurate manner whilst yielding a highly tractable model.

Each node has a complete set of decision variables, subject to standard generator and storage constraints including minimum stable generation, maximum (dis)charge, state of charge limits and the power balance constraint:

$$\sum_{g \in G} P_g(n) + \sum_{s \in S} P_s(n) + \sum_{i \in I} P_i^{EV}(n) + P^w(n) - P^{wc}(n) + P^{sol}(n) - P^{solc}(n) = P^d(n) - P^{LS}(n) \quad (23)$$

There are also inter timestep constraints between nodes to define states of charge, plant commitment times and minimum up/down times. An exhaustive constraint list can be found in Section III of [18]. The probability of reaching a given scenario (node) weights the cost function:

$$\sum_{n \in N} \pi(n) \left(\sum_{g \in G} C_g(n) + \Delta\tau(n)(c^{LS} P^{LS}(n)) \right) \quad (24)$$

A rolling planning approach is used to simulate annual system operation. Decisions that minimise the expected operating cost

over the next 24h period are found. The decisions at the current root node are implemented and the system is rolled forwards by an hour, updating system states as well as wind and EV connectivity realisations. With this new information the scenario tree is updated and the process iterated.

III. EV CONNECTIVITY FORECASTING AND DATA ANALYSIS

Scheduling FR from aggregated V2G chargers requires forecasting the number of connected EVs. Accurate characterisation of the distributions of ΔN_i is important for two main reasons: 1) The analytical reformulations of (18) require knowledge of the true mean and std; and 2) The ΔN distributions inform ambiguity set selection.

Constraint (18), that translates the specified risk of under delivery to a scheduled amount of FR, is compatible with any forecasting technique that ascertains the mean and std of ΔN . Here, a simple forecasting technique using real data is adopted, where future connectivity is assumed well characterised by data from a similar time of the week during the previous year. This is to demonstrate how forecast outputs are translated into operational inputs. It is expected that in actual operation more advanced forecasting techniques will be employed.

A. Forecasting Technique

Real, open source EV fleet charging data [19] for 2017 is used to characterise two distinct fleets, 'domestic' and 'work'. The domestic fleet relates to 3.2m charging events across 25,000, 10kW chargers installed in people's homes. The work fleet relates to 103,000 charging events across 540, 20kW chargers installed in car parks of public sector buildings. A charging event records charge-point identity, EV connection and disconnection time. Most of the individual chargers only provided data for specific months of the year. To account for this, the number of active chargers each month was found, 'active' defined as at least 2 charge events per week. The true fleet size was then taken as the average number of active monthly chargers, 8,500 and 200 chargers for domestic and work respectively.

The domestic fleet is characterised by EVs disconnecting in the morning and then reconnecting in the afternoon. The work fleet exhibits the opposite trend during the week. Very few EVs connect to the work chargers on weekends. The connections and disconnections were grouped by hour to provide a yearly time series of $\Delta\hat{N}$, ΔN^{in} , ΔN^{out} , used in the constraints of Section II-C.

ΔN_i in (12) is the change in a fleet's number of connected EVs between the time of the scheduling decision (t_d), and during the scheduling time period (t_s). FR is an instantaneous net power injection, so intra-time-period connections must be considered. Thus the empirical distribution of ΔN_i is found by collating historical connectivity data assumed constant for 5 minute periods instead of hourly. The empirical distributions are then found by grouping the numbers by t_d and t_s , and whether it is a weekday or weekend.

The method used is demonstrated for the domestic fleet in Fig. 1. The historical EV connections from an example weekday morning are shown. The current time is $t_d = 07 : 00$, with

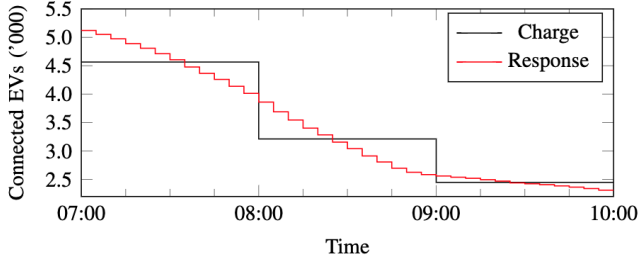


Fig. 1. Example of domestic EV connection values during a weekday morning with $N_0 = 5,119$, $t_d = 07:00$ and $t_s = 07:00 \rightarrow 08:00$ or $t_s = 08:00 \rightarrow 09:00$ or $t_s = 09:00 \rightarrow 10:00$. FR must consider intra-hour connections (5-min) to define ΔN_i , while charging decisions use average hourly values to define $(\Delta \hat{N})$.

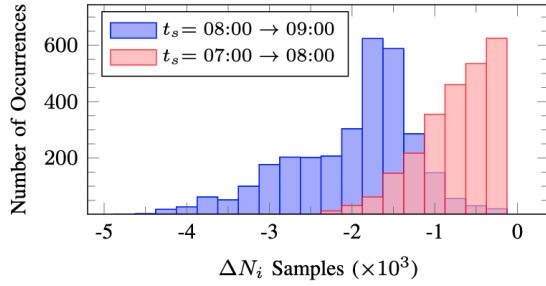


Fig. 2. Empirical distributions of ΔN_i for the domestic fleet on weekday, with $t_d = 07:00$ and $t_s = 07:00 \rightarrow 08:00$ or $t_s = 08:00 \rightarrow 09:00$.

$t_s = 07:00 \rightarrow 08:00, 08:00 \rightarrow 09:00, 09:00 \rightarrow 10:00$. The figure plots $\Delta \hat{N}$, average connection values that assume connections occur at the start of the time period then remain constant, used for energy and state of charge constraints. It also plots the ΔN values, when EV connection is assumed constant in 5 minute periods. This is needed when characterising the instantaneous power injection capability of the V2G chargers, and thus their FR capacity in (18).

The data from all the weekdays or weekends in the year grouped by t_d and t_s forms the empirical distributions of ΔN_i . The histograms for $t_d = 07:00$, $t_s = 07:00 \rightarrow 08:00$ and $t_s = 08:00 \rightarrow 09:00$ are plotted in Fig. 2. From these distributions the mean and standard deviation of each ΔN_i are found and input to (18).

The forecasting method is summarised as follows:

- 1) Group connections and disconnections by hour to provide a yearly time series of $\Delta \hat{N}, \Delta N^{in}, \Delta N^{out}$. Used in (21) and (22).
- 2) The net change in EV numbers between t_s and each 5 minute period within t_d is collected as a vector of length 12 for every day of the year ($\Delta N_{t_d, t_s}^{dd/mm}$).
- 3) $\Delta N_{t_d, t_s}^{dd/mm}$ are grouped by t_d and t_s to give the empirical ΔN_i distributions.
- 4) Extract the mean and standard deviation of ΔN_i for use in (18).
- 5) Apply statistical tests on ΔN_i distributions to choose correct ambiguity set.

B. Tests for Ambiguity Set Selection

The mean and standard deviation are necessary for all forms of (18) described by Table I, but sufficient for only the most

TABLE II
TESTS ON ΔN_i FOR NORMALITY AND UNIMODALITY

P-Value	< 0.05	0.05 : 0.50	0.50 : 0.95	> 0.95
Normality	19	12	12	5
Unimodality	0	0	7	41

conservative DRO form. If more distributional information of δ can be extracted from the distributions of its constituent ΔN_i , then the ambiguity set can be tightened, and (18) made less conservative.

We can establish the likelihood that the ΔN_i distributions conform to unimodal or Gaussian distributions by applying the Shapiro-Wilk and Hartigans dip test respectively. Because δ is the weighted sum of ΔN_i values, if they are established as Gaussian (and independent) with high likelihood, then so too is δ . Indeed, if the ΔN_i s can be shown to fit any distribution type with this summative property, then f_P^{-1} can be accurately defined as the inverse cumulative distribution function. The sums of unimodal distributions are likely to be unimodal [11], but not necessarily unimodal. Despite the lack of this mathematical guarantee, we show empirically in Section IV that a unimodal assumption within (18) can improve optimality whilst maintaining a significant conservative margin. Although to be guaranteed violation probabilities less than those specified, the DRO form must be implemented.

Table II shows the results from applying the Shapiro-Wilk and Hartigans dip test to the 24 weekday and 24 weekend ΔN_i distribution where the scheduling period is the hour immediately following t_d (i.e. $t_s = t_d \rightarrow t_d + 1$). These are chosen because the operational scheduling model used here optimally schedules for the entire next 24hr period every hour. Thus, when it makes its scheduling decision, it is only the one for $t_s = t_d \rightarrow t_d + 1$ that impacts reliability post fault, because the other decisions are subsequently revised to account for updated wind and EV connectivity realisations.

Typically the hypothesis (unimodality or normality) is rejected for p-values below 0.05 and accepted for values above 0.95. The hypothesis is neither rejected nor accepted for values between the two. Table II shows that the Gaussian hypothesis is not accepted, obvious from Fig. 2 due to the highly skewed distribution. On the other hand, 41/48 distributions are unimodal with high probability, with the other 7 being potentially unimodal.

IV. CASE STUDIES

The uncertainty-aware model for V2G proposed in this paper was incorporated into the SUC model introduced in Section II-D and used to identify how different EV fleet configurations impact the annual operational cost of the GB 2030 system. Generator and storage actions were optimally scheduled for 1 month of each season. A scenario tree that branches 7 times at the root node only was used to account for wind forecast uncertainty, which [18] showed to find the appropriate balance between tractability and optimality. Quantiles of 0.005, 0.1, 0.3, 0.5, 0.7, 0.9 and 0.995 were used. Unless otherwise stated, system generation and storage mix was as listed in Table III. Wind and solar generation output utilised historical data normalised between 0 and 1 to

TABLE III
GENERATION AND STORAGE CHARACTERISTICS

Generation	Nuclear	CCGT	OCGT
Number of Units	4	120	20
Rated Power (GW)	1.8	0.5	0.1
Min Stable Generation (GW)	1.60	0.25	0.05
No-Load Cost (£'000/h)	0.0	4.5	3.0
Marginal Cost (£/MWh)	10	47	200
Startup Cost (£'000)	NA	10	0
Startup Time (h)	NA	3	0
Min up Time (h)	NA	4	0
Inertia Constant (s)	5	4	4
Max Slow FR Capacity (GW)	0.00	0.05	0.04
Storage	Pumped	Battery 1	Battery 2
Capacity (GWh)	10	0.8	12
Dis/Charge Rate (GW)	2.6	0.4	3.0
Max Fast FR Capacity (GW)	0.0	0.8	0.0
Max Slow FR Capacity (GW)	0.5	0.0	0.0
Dis/Charge Efficiency	0.75	0.95	0.95

provide cross simulation consistency. Unless otherwise stated the installed capacity were 40GW and 20GW respectively. Historical demand data is used, scaled up to range between 20:60GW.

Current GB frequency security standards were used: $f_0 = 50$ Hz, $|\Delta f_{max}| = 0.8$ Hz and $RoCoF_{max} = 1$ Hz/s. The FR time constants are $T_1 = 1$ s, $T_2 = 10$ s, while $c_{LS} = £30,000/\text{MWh}$. Unless otherwise stated, two EV fleets were present on the system. With 85,000, 10 kW ‘Domestic’ V2G chargers and 15,000, 20 kW ‘Work’ V2G chargers. The parameters used were those derived in Section III, linearly scaled to match the total number. Nadir security was specified at 99%.

An eight-core Intel Xeon 2.40GHz CPU with 64GB of RAM was used to run simulations. The optimisations were solved using XPRESS 8.12 linked to a C++ application via the BCL interface. The mixed-integer program gap was 0.1%.

A. Constraint Reliability

Fig. 3 demonstrates how the specified risk of \bar{R}^{EV} under delivery (ϵ) compares to actual deliverability. This varies depending on the ambiguity set assumptions (Gaussian, unimodal or DRO) and the assumed true distribution of ΔN_i (Gaussian or empirical). Hourly nadir security (HNS) is the metric used to evaluate \bar{R}^{EV} deliverability. HNS for a specific hour is found by sampling the ΔN_i distribution for each fleet. When added to the number of currently connected EVs, the actual FR deliverable (R_j^{EV}) if an outage occurred at a random time over the scheduling period can be calculated. This process is repeated 100,000 times within each hour. The HNS is the cumulative ratio of $\bar{R}^{EV} > R_j^{EV}$. Fig. 3 shows only the t_s in the hour immediately following t_d . Due to the rolling planning approach of the SUC, the \bar{R}^{EV} values for other t_s are revised before the system would experience an outage.

When δ_n is assumed Gaussian and the R_j^{EV} is found from sampling Gaussian distributed ΔN_i , the HNS exactly equals the specified security level of 99% when constraint (18) is tight. The constraint is occasionally not tight during periods of high net demand when inertia and slow FR from thermal plants are sufficient to meet frequency security needs. During these time the HNS takes values above 99%. However, when

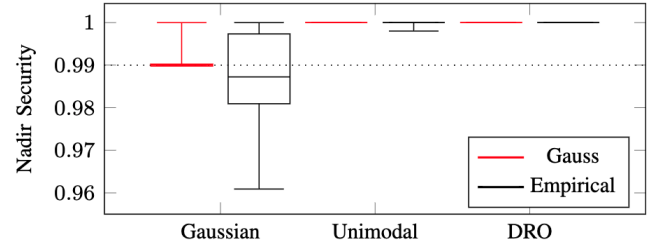


Fig. 3. The inter-quartile range, median and max/min of hourly nadir security levels under different ambiguity set assumptions (Gaussian, Unimodal, DRO) on δ when scheduling FR via (18). The scheduled amount was compared to true EV connectivity, found by sampling Gaussian or Empirical distributions of ΔN_i .

the true empirical ΔN_i distributions are sampled instead, 50% of hours have a HNS less than the specified 99%. In the worst period, using the Gaussian (18) constraint would result in only 96% of outages being contained securely. This unreliability is in line with the analysis of Table II, which showed none of the relevant empirical ΔN_i distributions are Gaussian. Thus using the Gaussian form of (18) is over optimistic and risks system security so is not considered further.

On the other hand, Fig. 3 shows that applying (18) assuming a unimodal or DRO δ_n distribution results in conservative HNS values for both the Gaussian and empirical distribution sampling. For Unimodal and DRO the worst periods have a HNS of 99.7% 99.9% respectively, with the majority of hours delivering more response than is scheduled with close to 100% probability. Again, this is in line with the analysis of Table II, which showed a high likelihood that ΔN_i are unimodal. It should be noted that the Gaussian distribution is a subset of the unimodal and DRO ambiguity sets, so is highly secured using both constraints.

B. Value of Response from V2G

The objective of deriving (18), the core contribution of this paper, is to enable a user to exploit the large operational gains from utilising the abundant EVs and V2G chargers in future systems to secure frequency. Crucially, the constraint is able to schedule response from these aggregated resources in a risk limited manner, despite their capacity being intrinsically uncertain. The ‘No V2G FR’ row in Table IV shows the status quo before this paper, where no response from distributed resources is scheduled. Zero FR is deliverable 100% of the time but offers no operational cost savings.

Alternatively a system operator could schedule FR using a simple deterministic approach, where it is assumed that the mean forecast number of EV connections will occur. This can be done by making $\sigma_i = 0 \forall i$ in (18), resulting in a linear constraint. By discounting uncertainty in this way, larger amounts of \bar{R}^{EV} are scheduled thus annual system costs are significantly reduced by £8,040/charger. However, because the mean is used, half of the time fewer EVs are available to provide response than is scheduled for. Thus this cost reduction comes at an unacceptable loss of nadir security, with average and worst case HNS being only 50%.

TABLE IV
CONSTRAINT VALUE COMPARISON FOR SPECIFIED 99% FREQUENCY
SECURITY AND 100,000 CHARGERS

Constraint	Worst Case Nadir Security	Charger Value (£/yr)	Charger CO ₂ Savings (tons/yr)
No V2G FR	100.0	0	0
DRO	99.9	5,760	33.6
Unimodal	99.7	6,330	37.4
Deterministic	50.0	8,040	44.5

The unimodal and DRO forms of (18) capture most of the cost savings of the naive deterministic approach (£633m/yr and £576m/yr respectively), whilst maintaining the high frequency security standards of the current ‘no FR from distributed providers’ approach. Since there are 100,000 chargers on the system, this translates into a substantial value of £6,330 and £5,760 per charger per year for unimodal and DRO respectively. Demonstrating that after accounting for the intrinsic uncertainty associated with FR from aggregated chargers using our tool, they remain an extremely valuable asset for future low inertia frequency control.

C. Investigating time-varying FR contribution from EVs

Fig. 4 shows how FR provision from aggregated EV fleets creates system value by significantly reducing wind and solar curtailment during low net-demand periods. It compares the operating conditions of the system with and without FR from EVs enabled over a typical 2-day period. The unimodal constraint is used. The net difference in committed CCGTs, wind and solar curtailment are plotted. Net demand is also plotted, this is equal to the total wind and solar energy available subtracted from demand, so is the same for both systems. The crucial difference is in how much more of this available zero marginal cost and emissions-free renewable power the system with FR from V2G is able to integrate.

During the first day, net demand is above 10 GW. The inertia from CCGTs committed to serve this load in combination with system FR is enough to fully secure frequency so no wind shed occurs in either system. However, during the second night demand drops and wind energy increases, resulting in low (and even negative) net-demand for the second day. In the system without FR from V2G, the inertia from thermal plants needed for energy provision alone is insufficient to secure the nadir (9). Consequently CCGTs must be committed for their inertia and FR alone. When the sum of the minimum stable generation of online thermal plants is larger than net demand, renewable power must be curtailed to respect the power balance constraint (23). The clear correlation between over commitment of CCGTs and wind curtailment is shown in Fig. 4.

Fig. 4 also plots the operation and FR provision of the domestic fleet during the same 2-day period. During the second night the EVs are charged at a constant rate. The need for full charge by morning synergises with the typically increased FR value overnight caused by lower net-demand. FR is a net power injection thus a charging EV can provide more response via demand alleviation. The approximately 0.6 GW of FR from the fleet during the second night replaces the inertia

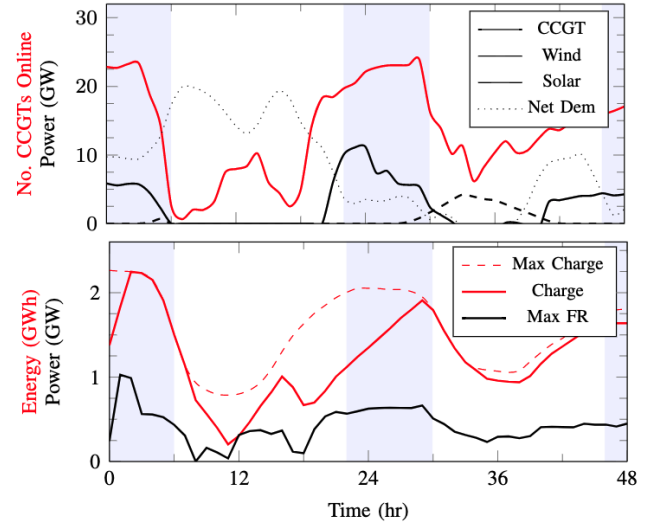


Fig. 4. Two day example comparing system operation with and without FR from V2G. Nighttime is shaded purple. The top figure plots the difference in: CCGT commitment number; wind and solar integration between the two systems. The bottom figure plots the operation of the Domestic fleet virtual battery for the system with V2G FR enabled.

from approximately 20 additional CCGTs, facilitating up to 11GW of wind integration. Cumulatively over the year the net difference in wind and solar curtailment amounts to 7.55 TWh and 0.40 TWh respectively. In other words, the highly effective FR from V2G connected EVs enables frequency secure operation at very low inertia levels, resulting in 8 TWh less power generated by burning fossil fuels (80 MWh per charger). This accounts for the majority of cost and emission savings in Table IV.

Finally, Fig. 5 plots the total \bar{R}^{EV} over the same 2 day period using deterministic, DRO and individual probability limited approaches. The latter approach ensures that the FR from each individual fleet is deliverable with 99% probability, achieved by applying (18) to each fleet (resulting in multiple linear constraints). This has less FR available than the DRO constraint, and thus less efficient operation. This is because the DRO constraint guarantees that the cumulative \bar{R}^{EV} is deliverable with at least 99% probability, explicitly accounting for the fact that on the rare occasion one fleet under delivers, the other fleets will likely over deliver to compensate. This efficiency gain increases with the number of fleets considered.

Another interesting observation from Fig. 5 is that the deterministic approach schedules much more response from EVs during the transitory morning and evening periods, but not overnight. This is because few cars connect overnight, thus the σ_i values are very low, and the FR capacity is thus known with high probability. This is advantageous as accounting for uncertainty does not significantly reduce the FR available during the valuable low net demand periods at night.

D. Value's Sensitivity to User Risk aversion and Forecast Uncertainty

A useful feature of (18) is that it that it directly translates a user's risk aversion level (ϵ) into a scheduled amount of FR. Fig. 6 illustrates that higher risk aversion leads to less response allowed from EVs and thus lowers their value. The

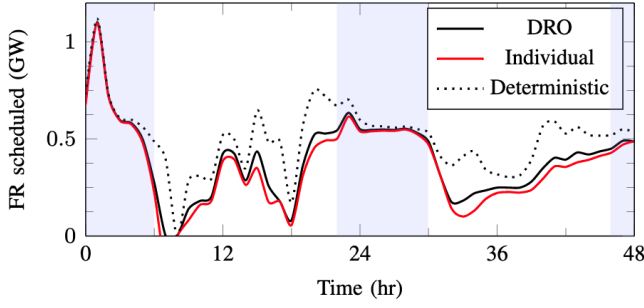


Fig. 5. The scheduled \bar{R}^{EV} over two days using deterministic, DRO and individual probability limited approaches.

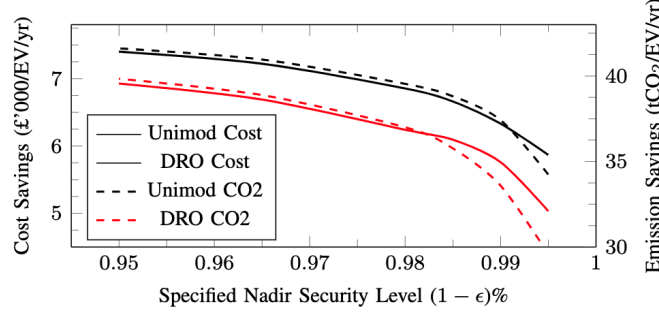


Fig. 6. Sensitivity of charger value to FR under-delivery risk aversion.

tightened ambiguity set from assuming δ_n is unimodal results in a larger $\frac{1}{f_P^{-1}(1-\epsilon)}$ constant in (18), and thus more \bar{R}^{EV} can be scheduled than the DRO case for the same ϵ . This explains the increased operation cost savings shown in both Table IV and Fig. 6.

A large σ_i of ΔN_i implies that the number of connected EVs in the scheduling period of interest is highly variable. This decreases the amount of schedulable FR from the chargers because a high deliverability probability necessitates covering the edge cases where far fewer EVs than the mean are connected at the time of an outage. A reduced std has the opposite effect, increasing the amount of schedulable FR, this is reflected in Fig. 7 which shows how the V2G's value varies in relation to a multiplier applied to the stds in equation (18). As the stds tend to zero, the cost saving tends towards the deterministic case level of £8,000/yr, with the difference between DRO and unimodal ambiguity set assumptions diminishing. It is interesting to observe that even with very large stds the EVs still provide substantial value of approximately £2,000/yr because their connectivity variability overnight is very low (shown in Fig. 5), so FR provision during this valuable period is mostly uninterrupted.

The relationship between a small std and increased V2G value has two main implications for real life application of (18). Firstly, more accurate EV connectivity forecasting methods are directly incentivised. Secondly, closer to real time scheduling of FR is desirable as it facilitates reduces uncertainty in forecasting.

E. Value's Sensitivity to System Characteristics

The value of response from V2G is highly dependant on its ability to facilitate higher renewable integration by displacing

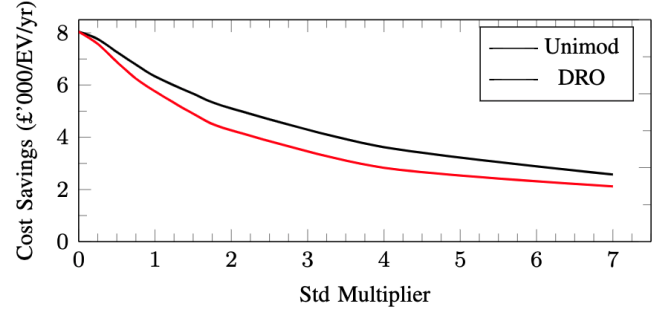


Fig. 7. Sensitivity of charger value to increased std of ΔN_i .

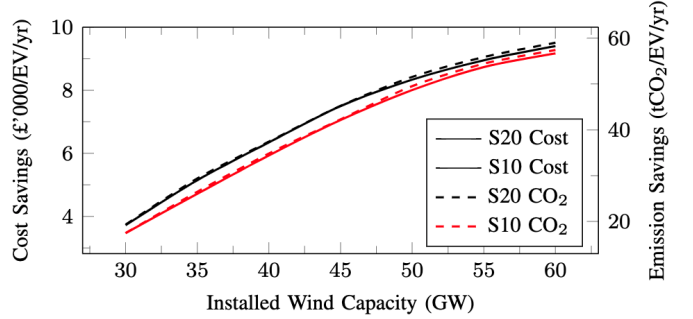


Fig. 8. The main value creation mechanism of FR from V2G chargers is the ability to facilitate renewable generation integration by displacing inertia and FR from thermal plants. The value sensitivity to installed system wind and solar (20GW or 10GW) capacity is plotted here.

the inertia and FR from thermal plants. Consequently, Fig. 8 shows that increased renewable generation increases V2G value. With 60 GW of wind and 20 GW solar one V2G charger has an annual system value of £9,400/yr. This comes from the increased frequency and magnitude of low-inertia periods, where the FR from the 100,000 chargers facilitate a cumulative 14.3 TWh of renewable power integration.

FR from V2G chargers competes with FR from grid batteries to create value, Fig. 9 compares their efficacy. It plots the operational cost increase incurred by applying the Nadir and RoCoF constraint to systems with different storage amounts. The unimodal constraint was used. Figure 9 shows that the first 2.50 GW of V2G capacity (i.e. 175,000 domestic, 37,500 work chargers) is approximately 30% as valuable to the system as the same battery capacity. For example to reduce frequency security cost to £1.5bil/yr requires 0.35 GW of batteries or 0.95 GW of V2G. Reduction to £0.75bil/yr requires 0.75 GW of batteries or 2.30 GW of V2G. Above 2.50 GW of V2G capacity, renewable shedding occurs due to the nadir constraint only during the highly uncertain morning period, examples of which are shown in Fig. 5. Increased capacity alleviates this slowly, whereas battery storage has no uncertainty so the same effect is not observed.

This derating of V2G capacity compared to batteries is primarily attributable to V2G not offering FR when EVs are not connected. From the fleet parameters derived in Section III, the average charger has an EV plugged in 42% and 26% of the time for 'Domestic' and 'Work' respectively. This is adjusted for within Fig. 9 with the average annual V2G capacity available plotted against value created for both the deterministic and unimodal constraints. The small difference

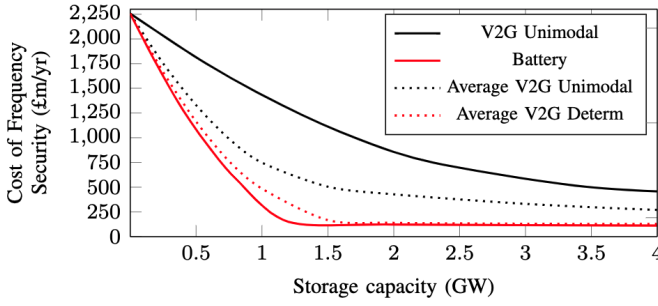


Fig. 9. Operational cost increase from applying the frequency security constraints to systems with different storage penetrations. The difference between battery and V2G is primarily because the chargers on average only have an EV connected (thus FR capability) $\approx 40\%$ of the time. Adjusting for this gives the ‘Average V2G’ capacity plots.

TABLE V
SENSITIVITY OF NORMALISED V2G VALUE TO FR PROVISION DELAY

Delay (s)	0	0.2	0.4	0.6	0.8	1.0
Normalised Value	1.00	0.97	0.93	0.89	0.85	0.80

between deterministic and the battery capacity is attributable to time of connection and charge requirements to meet energy needs. The difference between the unimodal and deterministic plots is due to uncertainty, revealing this to be the second most impactful derating factor. Uncertainty has low impact below 1 GW of average capacity, but above this it prohibits frequency security cost reduction. This suggests that the addition of a fleet with low morning plugin uncertainty, or a small amount of grid batteries would be valuable at high charger penetrations.

F. Impact of Delays on Value of EV's Response

All other sections of this paper assume FR from EVs begin ramping up the instant of PL_{max} disconnection. In reality, the triggering mechanism may involve delays caused by communication or frequency measurement requirements. The additional term in (10) allows the impact of delays on the value of FR from V2G connected EVs to be analysed within the SUC. The results are shown in Table V. The normalised value decrease is shown, this is the same for both the unimodal and DRO cases. Delays decrease the efficacy of response in containing frequency drop and thus reduce its value. Although, even when the final FR delivery time is doubled with a 1s delay, the value of FR remains substantial at £5,060/EV/yr for the unimodal case, or a decrease of 20% with respect to the case with no delay.

V. CONCLUSION AND FUTURE WORK

This paper proposes a mathematical framework to schedule frequency response from aggregated V2G chargers under uncertainty in EV plug-in times. A distributionally-robust chance constrained formulation for the frequency-security limits is introduced, compatible with any probabilistic forecast for EV connections and providing a convex feasible region. Case studies demonstrate that the proposed scheduling methodology facilitates large cost savings (\approx £6,000/charger) in the future Great Britain low inertia system due to displaced inertia and

FR requirements from thermal plants. Crucially, this value is obtained with mathematical guarantees on system frequency security.

In future, a model that accounts for charger location should be developed. Given the significant economic benefits that V2G could provide, it will be key to coordinate V2G power injections to ensure that distribution-side network constraints are respected. Secondly, the design of a market for FR that allows aggregator participation should be investigated. The tool developed here allows market clearing under security guarantees, but the mechanism of specifying, communicating and monitoring aggregator uncertainty characteristics needs development.

REFERENCES

- [1] F. Teng *et al.*, “Stochastic Scheduling with Inertia-Dependent Fast Frequency Response Requirements,” *IEEE Transactions on Power Systems*, vol. 31, no. 2, pp. 1557–1566, mar 2016.
- [2] L. Badesa *et al.*, “Simultaneous Scheduling of Multiple Frequency Services in Stochastic Unit Commitment,” *IEEE Transactions on Power Systems*, vol. 34, no. 5, pp. 3858–3868, 2019.
- [3] Climate Change Committee, “The UK’s transition to electric vehicles,” 2020.
- [4] C. O’Malley *et al.*, “Value of fleet vehicle to grid in providing transmission system operator services,” in *2020 Fifteenth International Conference on Ecological Vehicles and Renewable Energies*, 2020.
- [5] A. Thingvad *et al.*, “Value of V2G frequency regulation in Great Britain considering real driving data,” in *2019 IEEE PES Innovative Smart Grid Technologies Europe (ISGT-Europe 2019)*, 2019.
- [6] A. Hajebrahimi *et al.*, “Scenario-wise distributionally robust optimization for collaborative intermittent resources and electric vehicle aggregator bidding strategy,” *IEEE Transactions on Power Systems*, vol. 35, pp. 3706–3718, 2020.
- [7] X. Lu *et al.*, “A model to mitigate forecast uncertainties in distribution systems using the temporal flexibility of EVAs,” *IEEE Transactions on Power Systems*, vol. 35, pp. 2212–2221, 5 2020.
- [8] M. Amini and M. Almassalkhi, “Optimal Corrective Dispatch of Uncertain Virtual Energy Storage Systems,” *IEEE Transactions on Smart Grid*, vol. 11, no. 5, pp. 4155–4166, 2020.
- [9] Y. Zhang *et al.*, “Distributionally robust chance-constrained optimal power flow with uncertain renewables and uncertain reserves provided by loads,” *IEEE Transactions on Power Systems*, vol. 32, pp. 1378–1388, 2017.
- [10] A. Bagchi *et al.*, “Investigating impacts of storage devices on distribution network aggregator’s day-ahead bidding strategy considering uncertainties,” *IEEE Access*, vol. 9, pp. 120 940–120 954, 2021.
- [11] L. Roald *et al.*, “Security Constrained Optimal Power Flow with Distributionally Robust Chance Constraints,” pp. 1–8, 2015. [Online]. Available: <http://arxiv.org/abs/1508.06061>
- [12] W. Xie and S. Ahmed, “Distributionally robust chance constrained optimal power flow with renewables: A conic reformulation,” *IEEE Transactions on Power Systems*, vol. 33, pp. 1860–1867, 2018.
- [13] Y. Chen *et al.*, “A distributionally robust optimization model for unit commitment based on kullback-leibler divergence,” *IEEE Transactions on Power Systems*, vol. 33, pp. 5147–5160, 9 2018.
- [14] A. Zhou *et al.*, “A linear programming approximation of distributionally robust chance-constrained dispatch with wasserstein distance,” *IEEE Transactions on Power Systems*, vol. 35, pp. 3366–3377, 9 2020.
- [15] P. Kundur, *Power System Stability and Control*, 1st ed. McGraw-Hill Education, 1994.
- [16] H. Chavez *et al.*, “Governor rate-constrained OPF for primary frequency control adequacy,” *IEEE Transactions on Power Systems*, vol. 29, pp. 1473–1480, 2014.
- [17] L. Badesa *et al.*, “Optimal Portfolio of Distinct Frequency Response Services in Low-Inertia Systems,” *IEEE Transactions on Power Systems*, vol. 35, no. 6, pp. 4459–4469, 2020.
- [18] A. Sturt and G. Strbac, “Efficient stochastic scheduling for simulation of wind-integrated power systems,” *IEEE Transactions on Power Systems*, vol. 27, no. 1, pp. 323–334, feb 2012.
- [19] “Electric Chargepoint Analysis 2017: Domestic,” Department for Transport, Tech. Rep., Feb 2018. [Online]. Available: <https://www.gov.uk/government/statistics/electric-chargepoint-analysis-2017-domestic>